Supporting Information
For
Effect of Sc spatial distribution on electronic and ferroelectric properties of AlScN

Bipin Bhattarai,[a] Xiaoman Zhang,[b] Wangwang Xu,[b] Yijia Gu,[c] W.J. Meng,[b] Andrew C. Meng [a*]

[a]*Department of Physics and Astronomy, University of Missouri Columbia, MO 65211, U.S.A.*

[b]*Department of Mechanical and Industrial Engineering, Louisiana State University, Baton Rouge, LA 70803, U.S.A.*

[c]*Department of Materials Science and Engineering, Missouri University of Science and Technology, Rolla, MO 65409*

**Corresponding author: acmeng@missouri.edu*

Growth

AlScN thin films were grown in an UHV dc magnetron sputter deposition system with base pressure below 5×10^{-10} Torr. The deposition system consists of a growth chamber pumped by one turbomolecular pump and one cryogenic pump and a turbomolecular-pumped load-lock chamber. The growth chamber accommodates 75 mm sputter sources for Al (99.99%) and Sc (99.99%). Low resistivity As-doped n^+-Si(111) substrates, with diameter of 50 mm and resistivities in the range of 0.001-0.005 Ω-cm, were cleaned ultrasonically in acetone and ethanol, etched alternately in 10% (v/v) HF and 40% (v/v) HNO_3, blown dry with dry N_2, mounted onto a Mo holder, evacuated in the load-lock chamber, and transferred into the growth chamber. The front side of the Si wafers faced incoming vapor fluxes while the back side faced a SiC-based electric heater. The actual substrate temperature was calibrated through direct optical access infrared pyrometry, with the Si emissivity set at 0.68. The Si wafers were heated in the growth chamber to ~800 °C for 30 min prior to film deposition at the same temperature. Growths were carried out in an Ar/N_2 mixture, with the input Ar (99.999%) and N_2 (99.999%) flow rates of 20 and 6 sccm, respectively. The targets were sputtered in a dc mode, and a -40 V substrate bias was applied. Growth of AlScN films occurred with the Al and Sc targets operated at 1.2 A and 0.4 A target currents, respectively. After growth, the specimens were allowed to cool to room temperature before being transferred out of the growth chamber.

Materials Characterization

TEM samples were prepared using a ThermoFisher Helios G4 dual beam Xe plasma focused ion beam/scanning electron microscope (PFIB/SEM). Electron beam induced deposition of Pt, followed by ion beam induced deposition of Pt was used to protect the sample from the ion beam. The sample was thinned at successively lower accelerating voltages, with final thinning performed at 8 kV. Probe aberration corrected STEM was performed using the ThermoFisher Spectra 300 instrument at an accelerating voltage of 200 kV and a probe current of ~ 120 pA. The microscope is equipped with a Super-X EDS silicon drift detector system with 0.7 sr solid angle. The electron energy loss signal was collected with a Gatan

Ultrascan detector with camera length of 20 mm using a Gatan imaging filter (GIF) aperture of 2.5 mm with a collection semi-angle β of 41.7 mrad.

Computational Details

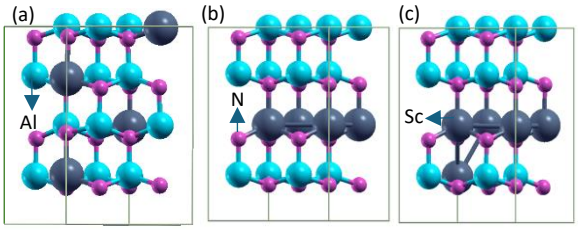

Figure S1 Supercells of $Al_{0.75}Sc_{0.25}N$ with (a) uniformly distributed Sc and (b) Sc clustered on a single basal plane; (c) $Al_{0.69}Sc_{0.31}N$ with 80% of Sc atoms clustered in a basal plane in addition 20% of Sc atoms pseudo-randomly distributed

All density functional theory (DFT) simulations of electronic structure[1] and electric polarization[2] were performed using the Quantum Espresso package.[3-5] Projector augmented wave (PAW) pseudopotentials were used to describe the core electrons; cutoff energy was set to 950 eV (70 Ry), charge density cutoff was set to 700 Ry, and k-point sampling was set to 4×4×4. DFT was implemented at the generalized gradient approximation (GGA) level with the PBE functional.[6] Electric polarization calculations in AlScN were carried out using a Berry phase method[2, 7] in the only *direction* (gdir =3) in which it is non-zero, along the c-axis with *number of k-points per each symmetry-reduced string* (nppstr) equal to 50. All structures are fully relaxed until the Hellmann-Feynmann forces in all the atoms of the cell are less than 10^{-6} Ry/Bohr. Furthermore, geometry optimization of the system is obtained with an energy convergence threshold of 10^{-6} Ry.

To test the effect of Sc distribution, AlScN crystals exhibiting Sc clustering in the basal plane are considered. We have constructed 1×1×8 and 1×2×4 supercells, each containing 32 atoms (16 Al, 16 N) to generate AlScN crystals in which one atomic plane consists entirely of Sc atoms for Sc concentrations of 6.25 and 12.5% respectively. Similarly, to generate AlScN crystals in which one atomic plane consists entirely of Sc atoms for 25% Sc-alloyed system, we have constructed a 2×2×2 supercell (also with 32 atoms). For AlScN supercells without Sc clustering in a basal plane, Al atoms are placed approximately uniformly (each Sc atom in a different basal plane). The details of both types of configurations are shown in Figure S1. We have used 2×2×2 supercells to study the properties of systems with approximately uniform Sc distributions

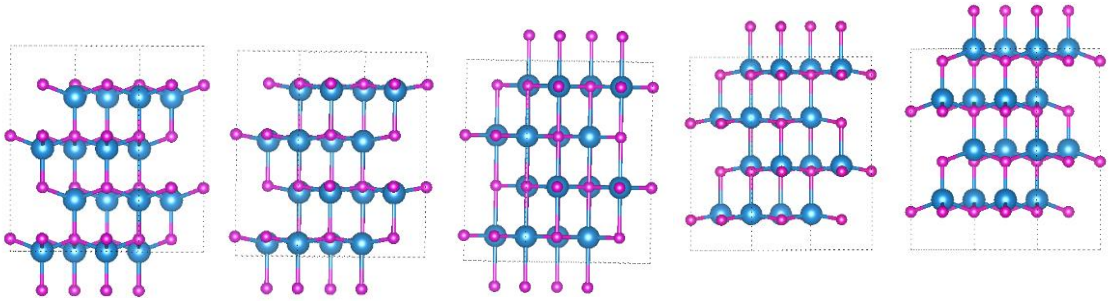

Figure S2. Virtual configurations of AlN from N-polar wurtzite to centrosymmetric h-BN to Al-polar wurtzite structures. The x and y coordinates of atoms are kept fixed, and z-coordinates are changed according to equation (1).

for all Sc compositions. For Sc concentrations greater than 25%, both in-plane and out-of-plane Sc clustering occurs (Figure S1c). Each AlScN supercell is fully relaxed before electronic structure and electrical polarization calculations are performed. A series of virtual states parametrizing the path from the relaxed WZ structure to the same structure with opposite polarity were constructed to sample the energy landscape during ferroelectric switching. These virtual states include the reference nonpolar centrosymmetric (CS) structure, which is created by distorting the WZ structure into the h-BN structure, as shown in Figure 3. In practice, this is accomplished by defining a parameter λ so that the u-parameter corresponding to the CS reference structure and the relaxed WZ structure gives λ = 0 and λ = 1, respectively, according to the mathematical formula below:

$$z_i(\lambda) = z_i^{CS} \pm (z_i^{WZ} - z_i^{CS})\lambda. \qquad (1)$$

In equation (1), $z_i(\lambda)$ is the z-coordinate of the ith atom in the unit cell in a λ state of distortion, and z_i^{CS} and z_i^{WZ} are the z-coordinates of the respective atoms in their centrosymmetric and wurtzite phases, respectively.

We have calculated the polarization values for each intermediate state to define the polarization branches, because the calculated spontaneous polarization is defined up to an integer multiple of polarization quantum.[8] In the present case, the final and the initial states are respectively the WZ and CS states of the system. If the calculated polarization for WZ structure ($\mathbf{P}_{WZ}$) falls on the nth branch, the value of required spontaneous polarization would be:[7]

$$P_s = \boldsymbol{P}_{WZ} + n\boldsymbol{P}_q - \boldsymbol{P}_{CS} \qquad (2)$$

Here, $\mathbf{P}_{CS}$ is the value of polarization calculated for the CS reference structure and $\mathbf{P}_q$ is the polarization quantum defined by $\boldsymbol{P}_q = \frac{e\boldsymbol{R}}{\Omega}$ with e, **R**, and Ω given by the electronic charge, lattice vector, and the volume of the unit cell respectively.

Results and Discussion

The calculated lattice parameters of relaxed pure AlN are a = 3.132 Å and c = 5.024 Å with the average internal structural parameter u = 0.381, which gives the ratio between the metal-nitrogen distance and the out-of-plane lattice constant, c. These values are consistent with the experimental results[9] (a = 3.110 Å, c = 4.980 Å, and u = 0.382). With increasing Sc content, the in-plane lattice parameter a is observed to increase monotonically while the c/a ratio decrease as shown in Figure 4. A similar trend has been reported in Sc alloyed AlN as long as the wurtzite phase is maintained.[10, 11] The value of the in-plane lattice parameter, a, in AlScN with Sc-rich planar clusters is slightly smaller than that of AlScN with no Sc clustering [Figure 4(a)] for all Sc concentrations. This may be due to the cumulative effect of the lateral strain induced in the basal planes each containing Sc atoms.

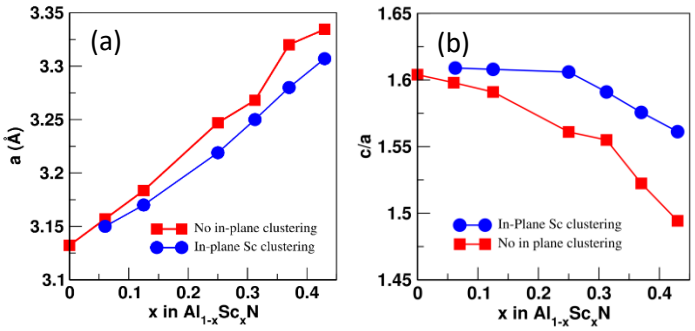

Figure S3 Effect of Sc concentration on lattice parameters of $Al_{1-x}Sc_xN$ for the systems with (a) no in-plane clustering, and (b) with in-plane clustering of Sc atoms.

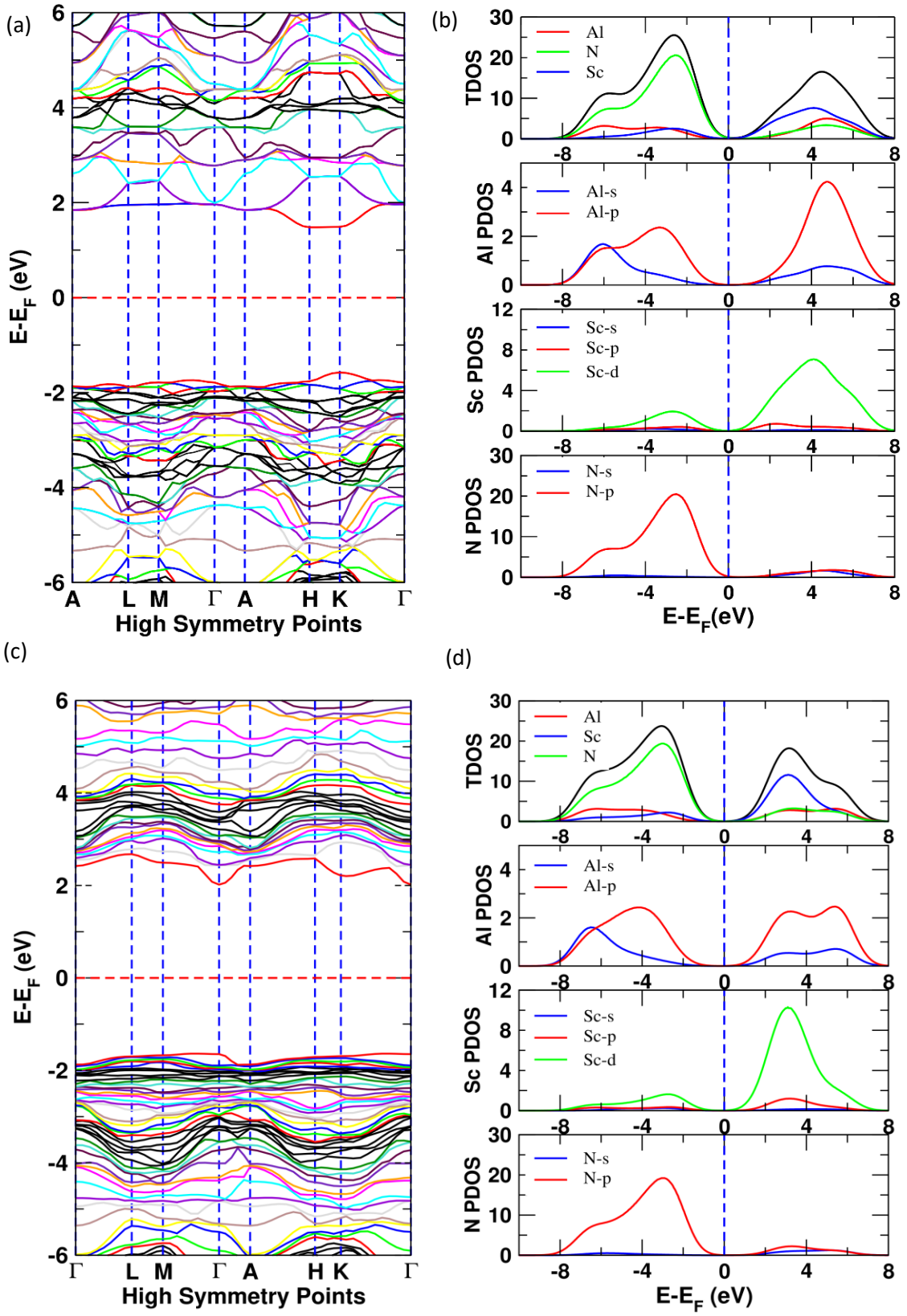

Figure S4 $Al_{0.75}Sc_{0.25}N$ (a) band structure and (b) density of states with basal plane Sc clustering; $Al_{0.75}Sc_{0.25}N$ (c) band structure and (d) density of states with approximately uniform Sc concentration.

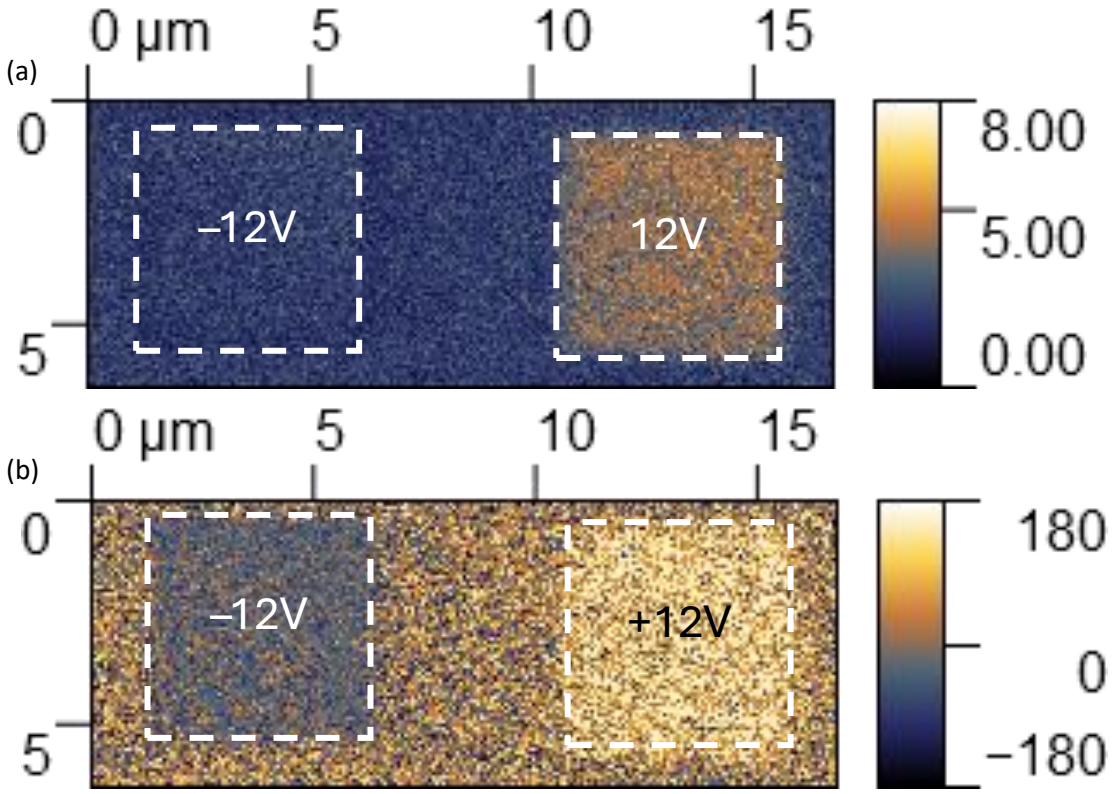

Figure S5 Piezoresponse force microscopy (PFM) poling on AlScN thin films grown at 550°C showing piezoresponse a) amplitude and b) phase changes due to DC poling at ±12V

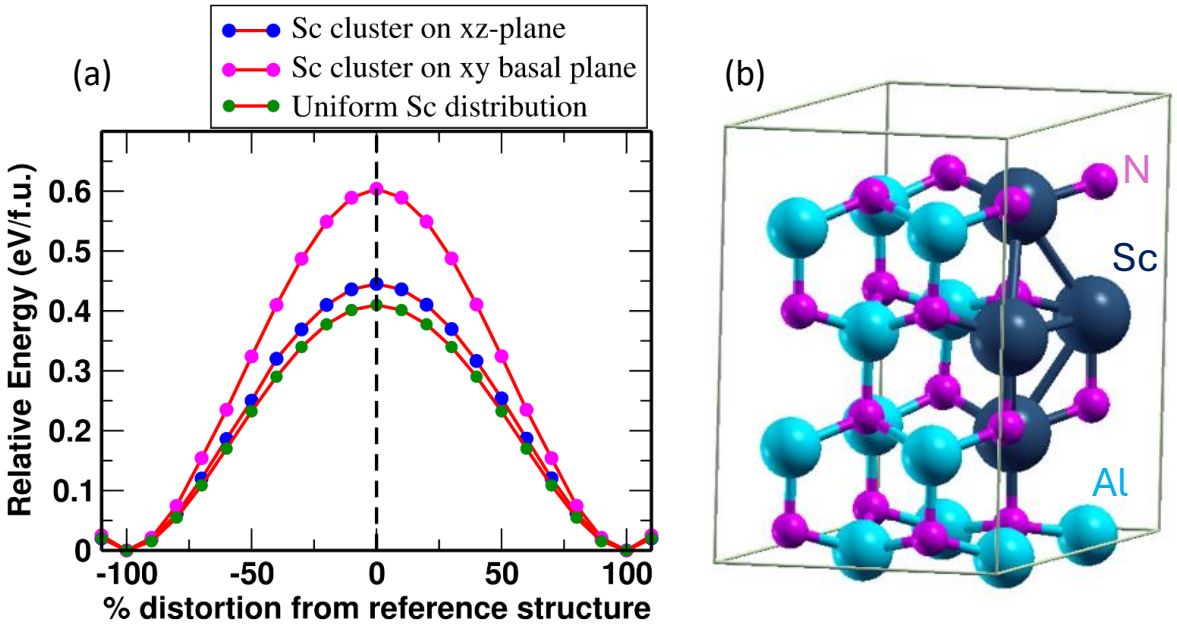

Figure S6 a) Comparison of increase in ferroelectric switching barrier due to Sc clustering in the basal plane and perpendicular to the basal plane in reference to a pseudo-uniform Sc distribution; b) schematic of Sc clustering geometry perpendicular to the basal plane

References

1. P. Hohenberg and W. Kohn, *Phys. Rev.*, 1964, **136**, B864-B871.
2. R. Resta, *J. Phys. Condens. Matter*, 2010, **22**, 123201.
3. P. Giannozzi, S. Baroni, N. Bonini, M. Calandra, R. Car, C. Cavazzoni, D. Ceresoli, G. L. Chiarotti, M. Cococcioni, I. Dabo, A. Dal Corso, S. de Gironcoli, S. Fabris, G. Fratesi, R. Gebauer, U. Gerstmann, C. Gougoussis, A. Kokalj, M. Lazzeri, L. Martin-Samos, N. Marzari, F. Mauri, R. Mazzarello, S. Paolini, A. Pasquarello, L. Paulatto, C. Sbraccia, S. Scandolo, G. Sclauzero, A. P. Seitsonen, A. Smogunov, P. Umari and R. M. Wentzcovitch, *J. Phys. Condens. Matter*, 2009, **21**, 395502.
4. P. Giannozzi, O. Andreussi, T. Brumme, O. Bunau, M. Buongiorno Nardelli, M. Calandra, R. Car, C. Cavazzoni, D. Ceresoli, M. Cococcioni, N. Colonna, I. Carnimeo, A. Dal Corso, S. de Gironcoli, P. Delugas, R. A. DiStasio, A. Ferretti, A. Floris, G. Fratesi, G. Fugallo, R. Gebauer, U. Gerstmann, F. Giustino, T. Gorni, J. Jia, M. Kawamura, H. Y. Ko, A. Kokalj, E. Küçükbenli, M. Lazzeri, M. Marsili, N. Marzari, F. Mauri, N. L. Nguyen, H. V. Nguyen, A. Otero-de-la-Roza, L. Paulatto, S. Poncé, D. Rocca, R. Sabatini, B. Santra, M. Schlipf, A. P. Seitsonen, A. Smogunov, I. Timrov, T. Thonhauser, P. Umari, N. Vast, X. Wu and S. Baroni, *J. Phys. Condens. Matter*, 2017, **29**, 465901.
5. P. Giannozzi, O. Baseggio, P. Bonfà, D. Brunato, R. Car, I. Carnimeo, C. Cavazzoni, S. de Gironcoli, P. Delugas, F. Ferrari Ruffino, A. Ferretti, N. Marzari, I. Timrov, A. Urru and S. Baroni, *J. Chem. Phys.*, 2020, **152**.
6. J. P. Perdew, K. Burke and M. Ernzerhof, *Phys. Rev. Lett.*, 1996, **77**, 3865-3868.
7. L. D. Filip, N. Plugaru and L. Pintilie, *Model. Simul. Mater. Sci. Eng.*, 2019, **27**, 045008.
8. N. A. Spaldin, *J. Solid State Chem.*, 2012, **195**, 2-10.
9. H. Schulz and K. H. Thiemann, *Solid State Communications*, 1977, **23**, 815-819.
10. K. Furuta, K. Hirata, S. A. Anggraini, M. Akiyama, M. Uehara and H. Yamada, *J. Appl. Phys.*, 2021, **130**.
11. H. Wang, N. Adamski, S. Mu and C. G. Van de Walle, *J. Appl. Phys.*, 2021, **130**.